

Digital Discovery

Accepted Manuscript

This article can be cited before page numbers have been issued, to do this please use: R. J. Appleton, B. C. Barnes, S. F. Son and A. Strachan, *Digital Discovery*, 2025, DOI: 10.1039/D5DD00422E.



This is an Accepted Manuscript, which has been through the Royal Society of Chemistry peer review process and has been accepted for publication.

Accepted Manuscripts are published online shortly after acceptance, before technical editing, formatting and proof reading. Using this free service, authors can make their results available to the community, in citable form, before we publish the edited article. We will replace this Accepted Manuscript with the edited and formatted Advance Article as soon as it is available.

You can find more information about Accepted Manuscripts in the [Information for Authors](#).

Please note that technical editing may introduce minor changes to the text and/or graphics, which may alter content. The journal's standard [Terms & Conditions](#) and the [Ethical guidelines](#) still apply. In no event shall the Royal Society of Chemistry be held responsible for any errors or omissions in this Accepted Manuscript or any consequences arising from the use of any information it contains.

A Deep Learning Approach to Searching Property Spaces of Materials

Robert J. Appleton¹, Brian C. Barnes², Steven F. Son³, Alejandro Strachan^{1*}

¹ School of Materials Engineering and Birck Nanotechnology Center, Purdue University, West Lafayette, Indiana 47907, USA

² U.S. Army Combat Capabilities Development Command Army Research Laboratory, Aberdeen Proving Ground, Maryland 21005, USA

³ School of Mechanical Engineering, Purdue University, West Lafayette, Indiana 47907, USA

Abstract

Melt processing of molecular crystals has several advantages over alternative routes for manufacturing materials such as pharmaceuticals, organic photovoltaics, and energetic materials. The experimental characterization of the materials properties required to assess melt processability (melting temperature, boiling temperature, decomposition temperature and vapor pressure) for the 1.3 million known molecular crystals is unfeasible; in fact, our survey of the research literature and open databases resulted in only 43 molecular materials with experimentally measured properties that satisfy a common criterion for melt-casting. We developed multi-task, graph-based neural network models that simultaneously predict these properties using a molecular graph as the only input. Screening databases of known molecules with our ML model resulted 2,532 melt-castable candidates, with melting temperature between 343K and 393K, boiling and decomposition temperature greater than 453K, and vapor pressure less than 0.0005 mmHg. Going beyond the space of known molecules, we apply our model with a generative approach to the CHNO chemical space, we discover 55,745 additional novel candidates with promising melt-castable characteristics. This three-orders-of-magnitude expansion highlights the power of coupling ML screening and generative design to accelerate materials discovery.

* Corresponding Author: strachan@purdue.edu



1. Introduction

Melt processing techniques, such as melt-casting and melt crystallization, are widely used for manufacturing various types of materials, including metals,¹ polymers,² and molecular crystals.³ Advantages of these methods include near-final shape production that minimizes the need for extensive machining that, in turn, leads to a reduction of material waste and processing time.^{4,5} In addition, controlled solidification can lead to uniform microstructures with fewer defects such as porosity, inclusions, and cracks, enhancing mechanical properties.⁶ Finally, melt-casting enables the production of components with intricate geometries that are difficult or impossible to achieve with traditional subtractive manufacturing methods making it a desirable method for biomedical implants,⁷ controlled drug delivery^{8,9} and solid-state batteries.¹⁰ Specific melt-cast applications for organic materials include organic glasses for high-efficiency scintillators,¹¹ organic thin-film transistors,¹² small molecule organic photovoltaics¹³ and energetic materials.^{14–16} The popular over-the-counter drugs ibuprofen and acetaminophen are prime examples where melt-casting has led to enhanced pharmaceutical characteristics, enabling faster, solvent-free production while also improving drug delivery, taste-masking, and controlled release.^{17–21} Unfortunately, a small fraction of molecular materials are melt-castable due to the multiple constraints on underlying properties. Melt-castability is largely dependent on the thermal stability of the molten liquid. The melting temperature should be moderately low to reduce energy costs and prevent damaging other components, but it cannot be too low to prevent unwanted melting during transport, storage, or other stages of the manufacturing and transportation process. The range of melting temperatures for melt-casting can vary across applications and for this work, we use the common range of 343K to 393K to enable energy-efficient melting through steam heating.^{14,15,22} We note that this melting temperature criteria would not include the previously mentioned acetaminophen due to its higher melting temperature (441K).²³ The stability of the liquid phase must be ensured by high decomposition and boiling temperatures to prevent generating toxic fumes and reduce material loss. To ensure the thermal stability of the liquid phase, Benz et al.¹⁴ proposed a minimum stability criterion of 453K. Surveying experimental data for melting temperature,^{24,25} boiling temperature,²⁴ and decomposition temperature,^{26,27} we identified 329 known CHNOFCI molecules that satisfy the thermal stability criteria for melt-casting. However, the vapor pressure of the material should also be low and using a generous filter of <0.0005 mmHg reduces the list to only 43 CHNOFCI molecules with experimental measured properties that meet both the thermal stability and vapor pressure criteria. This estimate represents a lower bound as it was obtained based on available data in common public databases discussed below. We have listed the resulting known melt-castable materials from this survey in the supplemental material. In addition, this number does not include composite formulations designed to improve or enable melt-processing.

Gaps in available experimental measurements for known molecules can be bridged with machine learning (ML), and such data would be very valuable to guide experimental studies. The development of quantitative structure–property relationship (QSPR) models has been a



cornerstone of chemistry research since the 1940s²⁸ and has also played a role in other areas of the physical sciences.^{29–42} With the emergence of ML, QSPR modeling has expanded in scope and capability, enabling more accurate and data-driven predictions across a wider range of scientific domains. These models were originally developed using hand-crafted descriptors^{43,44} that attempted to capture important chemical and structural properties of a molecule that govern the corresponding property of interest.^{45–48} Modern deep learning approaches have implemented graph-based methods such as graph convolutional networks^{49–51} (GCNs) and message-passing neural networks^{52–57} (MPNNs) that can achieve higher accuracy for property prediction than their QSPR predecessors. In this work, we trained a directed-message passing neural network (D-MPNN)^{52,53} to predict fundamental properties for determining melt-castability of molecular crystals from the corresponding gas-phase molecular graph. Using our ML model, we screened molecules based on thermal stability and vapor pressure and identified 2,532 known molecules predicted to be melt-castable.

Beyond screening known molecules, we utilized a generative approach to explore property spaces and discover novel melt-castable materials. Deep generative methods for inverse design in molecular and materials science have been widely studied over the last decade, including variational autoencoders (VAEs),^{58–68} generative adversarial networks (GANs),^{69–71} and diffusion models.^{72–75} A key challenge in molecular and materials discovery is generating candidates that are both synthesizable and processable. In metallic alloys, computational phase diagram (CALPHAD) approaches, often parameterized using large datasets of first-principles formation energies^{41,76} and convex hulls^{77–79} calculations, are routinely used to identify thermodynamically stable structures with accessible processing conditions.⁸⁰ In contrast, melt-castability of molecular crystals depends on multiple thermophysical properties, motivating the deep-learning-based, multi-property screening and generative strategy adopted in this work.

Deep generative methods have proven successful at generating novel structures with ideal properties but require large datasets and expensive training. Metaheuristic optimization algorithms, such as genetic algorithms (GAs), have a longer history in molecular design.^{81–83} These methods can operate on the molecular graph or string representations such as simplified molecular-input line-entry system (SMILES)^{84,85} and typically require evolutionary operations with expert chemical rules to ensure generated molecules are valid.^{86–89} Self-referencing embedded strings (SELFIES),⁹⁰ a recently-proposed replacement for SMILES, is a robust string representation where every SELFIES string corresponds to a valid molecule. This representation led to the development of the STONED⁹¹ method for efficient and rule-free mutation and crossover operations in chemical space. Shortly after, JANUS-GA⁹² was introduced, it uses these genetic operators to enable inverse molecular design that is competitive with deep generative methods without the need for extensive training. In this work we extend JANUS-GA to incorporate Pareto-awareness and apply it to the discovery of novel melt-castable materials. We generate 55,940 molecules predicted to be melt-castable, 55,745 of which are not reported in the PubChem⁹³ or CAS SciFinder⁹⁴ databases and are likely new.



2. Methods

2.1 Data

We compiled a large dataset of experimental melting temperatures (T_m), boiling temperatures (T_b), decomposition temperatures (T_d) and vapor pressures (P_v) for known CHNOFCl materials. Data sources include the PHYSPROP database²⁴, the Jean-Claude Bradley Open Melting Point Dataset (JB OMPD)²⁵, and decomposition temperature data published in open literature^{26,27}, see details in Table 1.

Table 1: Summary of property data obtained from literature.

Property (units)	Number of Datapoints
Melting temperature, T_m (K) ^{24,25}	22,015
Boiling temperature, T_b (K) ²⁴	4,476
Vapor Pressure, P_v (mmHg) ²⁴	2,166
Decomposition temperature, T_d (K) ^{26,27}	637

For all molecules, SMILES strings were canonicalized using RDKit.⁹⁵ We removed cocrystals/mixtures and molecules with radicals. Duplicates were identified, and for multiple measurements of the same property, the median was used for training. We use the \log_{10} of the vapor pressures to account for the fact that the values span several orders of magnitude (10^{-10} - 10^5), this is consistent with previous works.^{29,96}

2.2 Property Prediction Model Design

The multi-task (MT) ML model for property prediction was developed using the *chemprop* framework,^{52,53} an implementation of a directed message-passing neural network (D-MPNN) for predicting properties from the molecular graph. To evaluate the model performance, we use a 5-fold cross-validation scheme. Specifically, we trained five separate models (one for each fold) and assessed the performance of each model on a corresponding test set that was not used in its training. Upon deployment, the models are used as an ensemble where the prediction is taken as the mean of the five models, and the uncertainty is the standard deviation. The values for each property are scaled using a standard scaler before training to address the fact that the properties have different ranges of magnitude. Hyperparameters were optimized minimally by adjusting the size of the network and other training details for the D-MPNN are provided in Table S1 of the supplemental material. Similar models built with this framework have proven successful for these properties in previous works.^{26,57,96}

2.3 Genetic Algorithm for Molecule Generation

The generative approach used in this work is built on the JANUS-GA framework.⁹² JANUS-GA is a GA designed for inverse molecular design, employing a parallel-tempering-inspired^{97,98}



framework with two distinct populations: one for global exploration and another for local exploitation. We describe the algorithm briefly here and refer the readers to the original publication⁹² and the supplemental material for additional details. A fitness function is used to evaluate the members of both exploration and exploitation populations and the 5 top ranked individuals in each population are shared. The explorative population is subject to both mutation and crossover operations. This step generates an “overflow of potential children” and uses a deep neural network (DNN) to down sample molecules to maintain a fixed population size. The exploitative population refines promising molecular candidates using mutations based primarily on molecular similarity. JANUS-GA leverages the SELFIES molecular representation and the STONED algorithm to generate new molecules,⁹¹ bypassing the need for manually defined structure-validation rules. We extended the JANUS-GA for dual-property optimization using both the change in area under the Pareto front and their combination into a single objective function. We study different combinations of Pareto front and single objective function as the fitness function and for overflow down-sampling, both using a pre-trained MT D-MPNN. The implemented Pareto-aware fitness evaluation is described in Algorithm 1 below.

Algorithm 1: Pareto-Aware Fitness Evaluation in JANUS-GA

Input: Population of molecules with two property values and number of generations, G

Output: Final population of molecules

```

1  while ( $i < G$ ) do
2      Identify 2-d Pareto front from current population  $p_i$  and fit step function  $S$ 
3      for each molecule  $x$  in population  $p_i$  do
4          Compute Euclidean distance  $d$  to step function  $S$ 
5          if  $x$  is within  $S$ 
6               $fitness(x) = -|d|$ 
7          else
8               $fitness(x) = |d|$ 
9          end if
10     end for
11     Select top  $k$  molecules with highest  $fitness$  and generate new molecules  $n$ 
12     Add new molecules to population,  $p_{i+1} = p_i + n$ 
13 end while

```

Using these modifications, we can push the 2D Pareto front equally on all fronts or along a preferred region by combining the two variables into a single objective function. This was motivated by our observation in preliminary work where Pareto optimization alone can lead to trivial solutions, Figure S2 of the supplemental material. Also, we implemented functions for collecting ensemble predictions from our MT D-MPNN models. The properties predicted by the



D-MPNN are used for identifying the Pareto front and computing fitness functions for new molecules but can also be used by the filters. Predictions come from the five different models trained on each of the 5-folds during cross validation. We record the mean and standard deviation of each property across these models. Previous work found that using a DNN to down sample the explorative population leads to populations with higher median fitness.⁹² In this work, the DNN is replaced with an objective function using actual predictions from our ML models. In the original implementation of JANUS-GA,⁹² the DNN serves as a surrogate for the fitness function, aiming to reduce the number of potentially expensive fitness evaluations by leveraging model predictions. In contrast, our implementation uses the same ML model for both down-sampling and fitness evaluation, resulting in no computational savings since the evaluation cost remains unchanged. The source code for the modified JANUS-GA is available at <https://github.com/R-applet/JANUS> and a summary of the algorithm parameters used in this work is provided in Table S2 of the supplemental material.

3. Results

3.1 Property Model Performance

Figure 1 shows the MT model predictions compared to the experimental values for the testing data of each property. We find that the model predictions for boiling temperatures (T_b) and vapor pressures (P_v) are in exceptional agreement with experiment with $R^2 > 0.9$. The model predictions for melting temperatures (T_m) are slightly less accurate with $R^2 = 0.84$ with MAE and RMSE values comparable to previous works that looked at similar datasets for slightly different chemical spaces.^{26,99} We note that the performance of our model on decomposition temperatures (T_d) is poor with $R^2 = 0.56$. The MAE and RMSE on T_d are consistent with previous reports on this dataset.²⁶ The limitation of our model reflects the data scarcity and for experimental T_d data. In our usage of the model, we are looking to maximize the decomposition temperature, not try to predict a specific value, therefore the model predictions are strong indicators for thermal stability. For these reasons, we believe our model can be used to estimate both thermal stability and volatility. The validation learning curves for each fold are shown in Figure S1 of the supplemental material. Using this model to make predictions on the materials within the experimental data used to develop the model, we are able to fill the gaps for the measured properties. Screening this completed dataset, we identify 2,532 known molecules predicted to be melt-castable. The list of these materials and their associated predicted properties are provided in the supplemental material and experimental efforts to validate these predictions would be highly valuable.



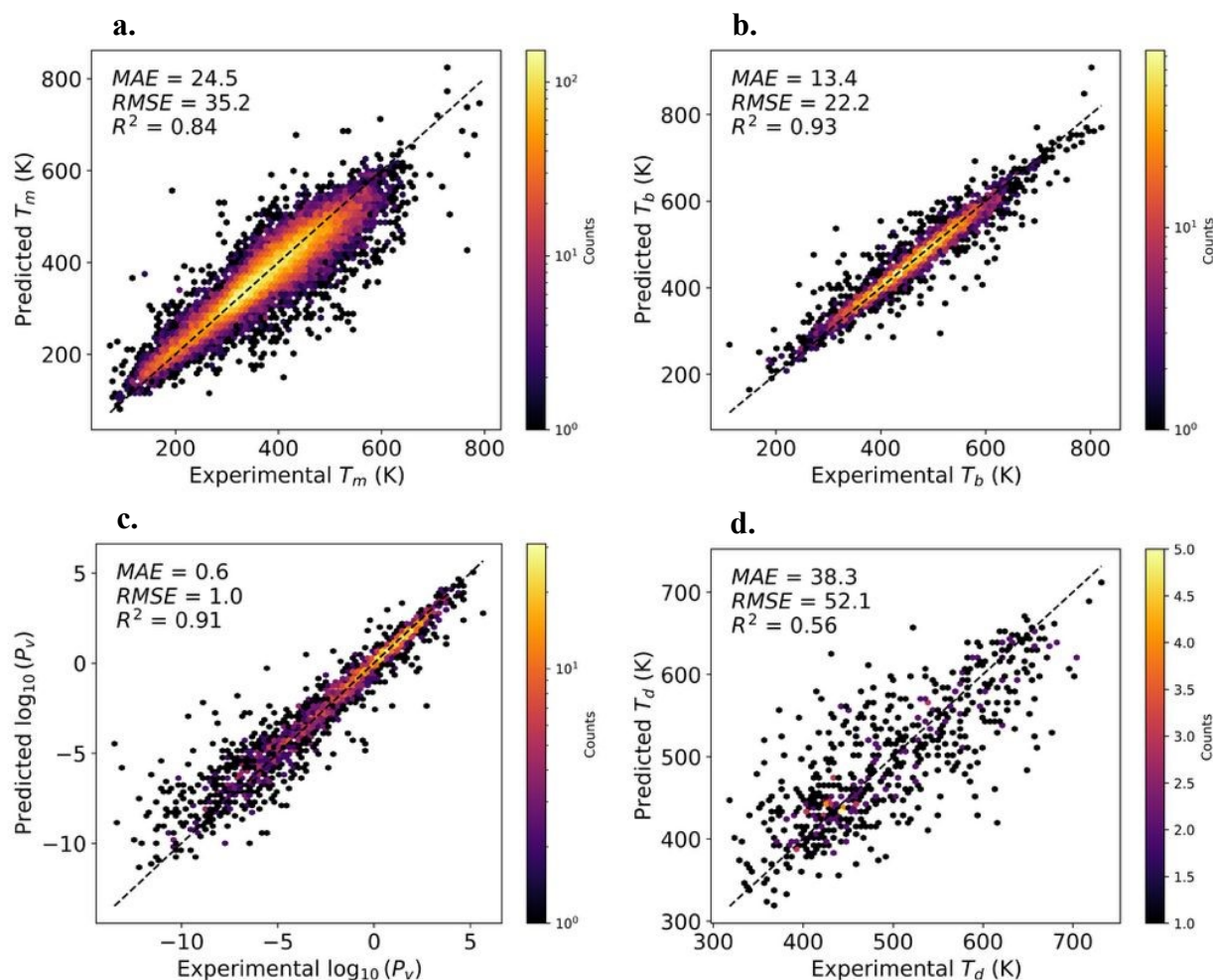


Figure 1. Parity plots for the test predictions across 5-fold cross validation for melting temperature (a), boiling temperature (b), vapor pressure (c) and decomposition temperature (d). Each prediction corresponds to the model fold in which the data point was included in the test set, ensuring strict separation between training and evaluation.

3.2 Generation of molecules with high melt casting potential

We use the modified JANUS-GA⁹² to explore property spaces of CHNO molecules to generate novel molecules with ideal properties for melt-casting. Specifically, we sought to find new molecules that maximize the liquid stability range, minimize the distance from the ideal melting temperature, and minimize the volatility. The liquid stability range (ΔT_{liq}), is the temperature interval between the predicted melting temperature and whichever is lower, the predicted decomposition temperature or the predicted boiling temperature:

$$\Delta T_{\text{liq}} = \min(T_d, T_b) - T_m \quad (1)$$



The distance from the ideal melting temperature (ΔT_{im}) is the absolute difference between the predicted melting temperature and the provided ideal melting temperature (taken as 368K, which is the midpoint between 343K and 393K):

$$\Delta T_{im} = |T_m - 368| \quad (2)$$

To discover melt castable molecules, we explored two approaches: i) in the first we consider the Pareto front formed by ΔT_{liq} and ΔT_{im} , ii) the second approach considers vapor pressure and ΔT_{liq} and limits the search to desirable values of ΔT_{im} .

Liquid stability range and ideal melting temperature. In our first class of experiments (Pareto front formed by maximizing ΔT_{liq} and minimizing ΔT_{im}) we initialized our population by selecting CHNO molecules from the combined experimental dataset and require each molecule to contain carbon, nitrogen, and oxygen. We first discuss the impact of the use of Pareto front advancement vs. the single objective function for the fitness function and down-sampling. We performed three tests: Pareto fitness and objective down-sampling (denoted Pareto-Obj), objective fitness and objective down-sampling (denoted Obj-Obj), and Pareto fitness and random down-sampling (denoted Pareto-Rnd). The following objective function was chosen to favor molecules with low ΔT_{im} ,

$$O = \Delta T_{liq} - 3\Delta T_{im} \quad (3)$$

We evolved the population for 10 generations using a population size of 50 for both the exploitative and explorative populations. Each GA experiment was repeated 5 times to collect statistics. More details about the parameters of the GA are summarized in Table S2 and the results for the sampling experiments are shown in Section S4.1 of the supplemental material. In all cases, we discovered molecules that are highly thermally stable and push the ΔT_{liq} and ΔT_{im} Pareto front. To track the performance of the GA we plot the area under the Pareto front from each generation (the area is normalized such that the area in generation 0 is 1), see Figure 2(a). We find that the Pareto-Rnd GA pushes on a wide area of the Pareto front, while the Pareto-Obj and Obj-Obj GAs are highly localized with ΔT_{im} less than ~ 25 K. The advantage of using the objective function for down-sampling is that we generate more molecules that fall within the melting temperature range for melt-casting, as depicted by the fraction of melt-cast candidates per generation in Figure 2(b). Comparing the Pareto-Obj GA to the Obj-Obj GA we find that the Pareto-Obj GA results in a more converged Pareto front.



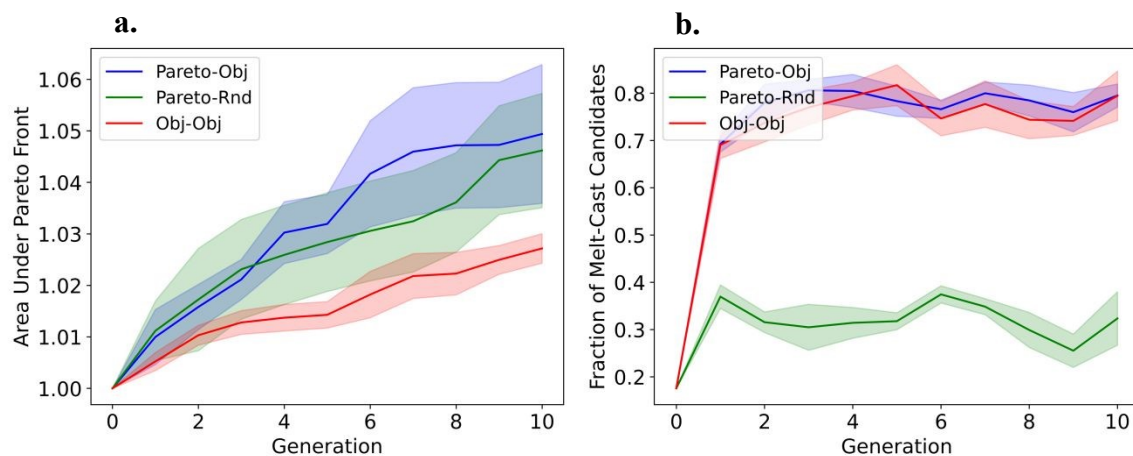


Figure 2. Evolution of the area under the Pareto front for optimizing ΔT_{liq} and ΔT_{im} (a) and Fraction of melt-cast candidates generated each generation (b). The solid lines represent the mean, and the shaded region represents the standard deviation across 5 independent experiments.

The results from the sampling experiments showed that the Pareto fronts generated were not converged and that running for more generations and larger generation sizes would continue to drive the Pareto front. On the other hand, there are hyperparameters of the GA that control the number of unique generated molecules and consequently the convergence and time for the GA to complete. We tested different hyperparameters of the JANUS-GA and evaluated how they influenced the evolution of the population. Specifically, we tested 3 different generation sizes (50, 100, and 200), using 5 random crossovers in the exploration population (default is 1), and 10% of the generation size as the number of mutations and number of random samples in the exploitation population (default is 400 for each). For each experiment, we tracked the number of unique molecules evaluated, unique molecules sampled in the population, and melt-cast candidates generated. We also report the wall time of each experiment. The results comparing the custom hyperparameters to the defaults are recorded in Table S3. Furthermore, we observed the distribution of each experiment and displayed them in Figure S5. The convergence by comparing the evolution of the area under the Pareto front across 25 generations displayed in Figure 3(a) and the distribution of ΔT_{liq} and ΔT_{im} for the generated molecules from the most converged GA is shown in Figure 3(b). For this set of experiments, the GA with a generation size of 200 and the default hyperparameters (1 random crossover in the exploration population and 400 mutations and random samples in the exploitation population) resulted in having the largest area under the Pareto front, see Figure 3(a).



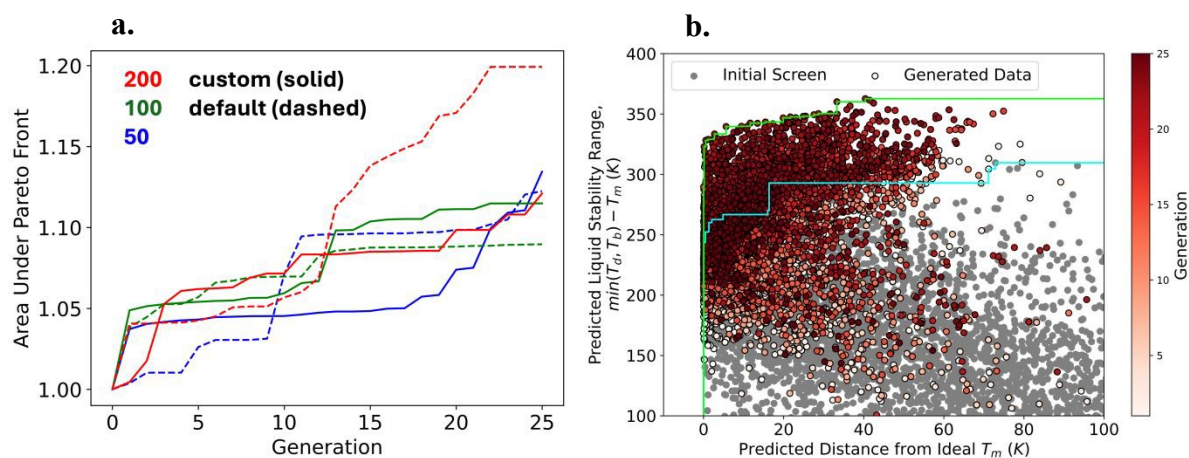


Figure 3. Evolution of the area under the Pareto front for optimizing ΔT_{liq} and ΔT_{im} (a) and the distribution of ΔT_{liq} and ΔT_{im} for CHNO molecules from literature (grey) and generated (red) (b). The Pareto front for the initial population is represented by the cyan step function and the Pareto front for the final population is represented by the lime green step function.

Observing the distributions of ΔT_{liq} and ΔT_{im} across the hyperparameter experiments (Figure S5), it is clear that using more mutations/random samples for the exploitative population leads to more points concentrated at the Pareto front. However, the consequence of using more mutations/random samples is that it generates a larger overflow of molecules and thus many more evaluations and a longer wall time, as shown in Table S3. We also note that even though more unique molecules were evaluated, we found fewer unique molecules were used in the population and typically less melt-castable candidates were discovered (with exemption of the runs with a population size of 100). We attribute this to the fact that more molecules are near the Pareto front and thus have high fitness leading to more individuals that are kept in the population and not replaced. In all cases, we are able to drive the Pareto front successfully and discover a large number of melt-castable candidates.

Liquid stability range and vapor pressure. In our second class of experiments (Pareto front formed by maximizing ΔT_{liq} and minimizing $\log_{10} P_v$), we

$$O = \Delta T_{liq} - 50 \log_{10} P_v(4)$$

The results for the sampling experiments for this case are shown in Section 4.2 of the supplemental material. In all cases, we can discover molecules with high thermal stability and push the Pareto front between ΔT_{liq} and $\log_{10} P_v$. In these experiments, we find the Pareto-Obj and Obj-Obj GAs push the Pareto front much further than the Pareto-Rnd GA, see Figure 4(a). Furthermore, the results for Pareto-Obj and Obj-Obj GAs are very similar for this set of experiments. Again, we find the Pareto-Obj and Obj-Obj GAs generate a larger fraction of melt-cast candidates per generation compared to Pareto-Rnd, see Figure 4(b). A clear inverse relationship is observed between ΔT_{liq} and $\log_{10} P_v$, where materials with wider liquid stability ranges generally exhibit lower vapor pressures, consistent with thermodynamic expectations



from the Clausius-Clapeyron relation.¹⁰⁰ The strong underlying correlations between ΔT_{liq} and $\log_{10} P_v$ makes this a much simpler optimization problem than optimizing ΔT_{liq} and ΔT_{im} . This explains why the difference between a Pareto-Obj driven GA and Obj-Obj driven GA is much less noticeable for the ΔT_{liq} and $\log_{10} P_v$ Pareto front. Furthermore, the Pareto-Rnd driven GA struggles to push the ΔT_{liq} and $\log_{10} P_v$ Pareto front because it is not taking advantage of the strong correlations.

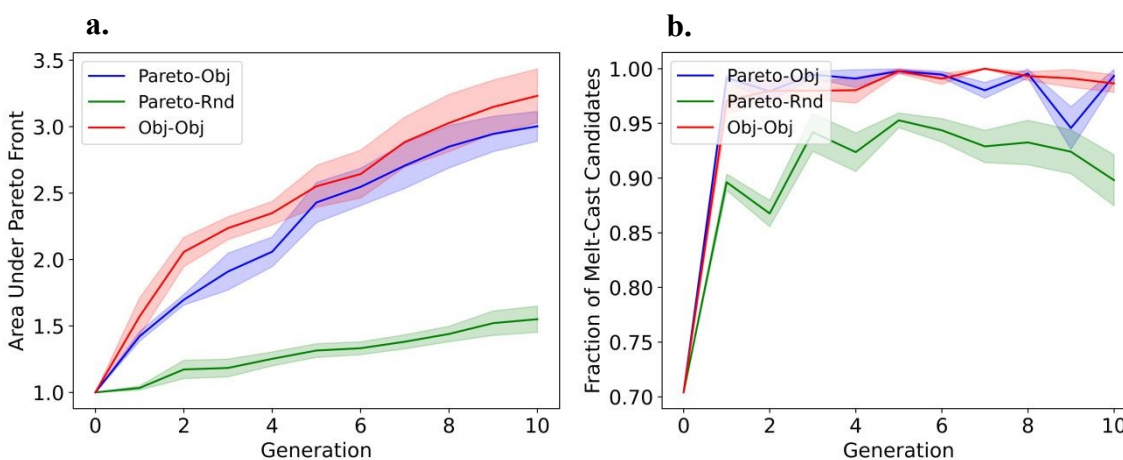


Figure 4. Evolution of the area under the Pareto front for optimizing ΔT_{liq} and $\log_{10} P_v$ (a) and Fraction of melt-cast candidates generated each generation (b). The solid lines represent the mean, and the shaded region represents the standard deviation across 5 independent experiments.

The results from the sampling experiments showed that the Pareto fronts generated were not converged and that running for more generations and larger generation sizes would continue to drive the Pareto front.

Similar to the previous set of experiments, we studied the hyperparameters and their effects on the evolution of the Pareto front. The results comparing the custom hyperparameters to the defaults are recorded in Table S4. Furthermore, we observed the distribution of each experiment and displayed them in Figure S6. The convergence by comparing the evolution of the area under the Pareto front across 25 generations displayed in Figure 5(a) and the distribution of ΔT_{liq} and $\log_{10} P_v$ for the generated molecules from the most converged GA is shown in Figure 5(b). For this set of experiments, the GA with a generation size of 200 and the custom hyperparameters (5 random crossovers in the exploration population and 20 mutations and random samples in the exploitation population) resulted in having the largest area under the Pareto front, see Figure 5(a).



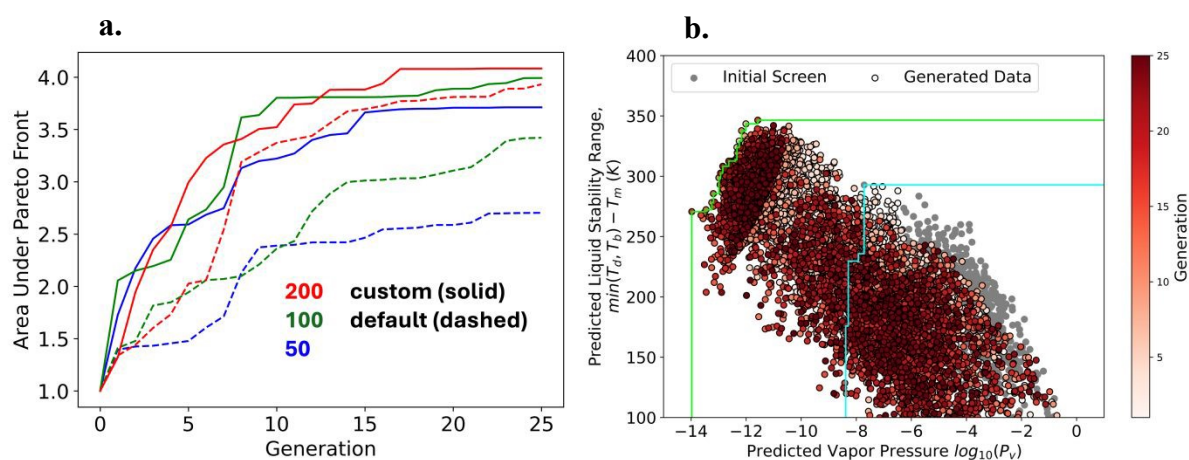
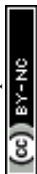


Figure 5. Evolution of the area under the Pareto front for optimizing ΔT_{liq} and $\log_{10} P_v$ (a) and the distribution of ΔT_{liq} and $\log_{10} P_v$ for CHNO molecules from literature (grey) and generated (red) (b). The Pareto front for the initial population is represented by the cyan step function and the Pareto front for the final population is represented by the lime green step function. All molecules plotted have a predicted melting temperature between 343K and 393K.

Observing the distributions of ΔT_{liq} and $\log_{10} P_v$ across the hyperparameter experiments (Figure S6), again we find that using more mutations/random samples for the exploitative population leads to more points concentrated at the Pareto front. Again, this corresponds to a larger overflow of molecules, more evaluations, and a longer wall time, as shown in Table S4. Consistent with the previous set of experiments, despite more unique molecules being evaluated, we found less unique molecules were used in the population and less melt-castable candidates were discovered. In all cases, we are able to drive the Pareto front successfully and discover a large number of melt-castable candidates.

4. Discussion

Across the populations in all simulations, we generated 62,082 unique molecules and 55,940 of these have predicted thermal stability and volatility to be considered a potential melt-castable material. From the 55,940 molecules, 195 were found to have been synthesized by searching PubChemPy,¹⁰¹ CIRpy¹⁰² and SciFinder.⁹⁴ We emphasize that these 195 molecules were not in the training set or initial population. These molecules confirm that our generative approach can discover real, synthesizable, molecules. Using SciFinder,⁹⁴ we obtained experimental melting temperatures for 58 of the 195 rediscovered molecules and plotted them against the model predictions in Figure S7 of the supplemental material to provide further validation of the model accuracy on unseen molecules. We find that the vast majority (51/58) of predictions fall within the model's test set RMSE (see Figure 1). Importantly, 61% of these molecules had experimental melting temperatures within the range to be melted via steam heating. This is further evidence that the model predictions are within the expected error.



The remaining 55,745 molecules have not been previously reported, based on our searches using PubChemPy,¹⁰¹ CIRpy¹⁰² and SciFinder.⁹⁴ To characterize the molecules generated, we computed the maximum Tanimoto similarity¹⁰³ of each new molecule to an extensive set of known molecules^{93,104} and also computed the synthetic accessibility score (SAscore).¹⁰⁵ The SAScores can be interpreted as 1 being “easy to make” and 10 being “very difficult to make” with the authors suggesting that molecules with SAScores greater than ~6 are difficult to synthesize.¹⁰⁵ Figure 6 we shows these values for the novel melt-cast molecules we generated.

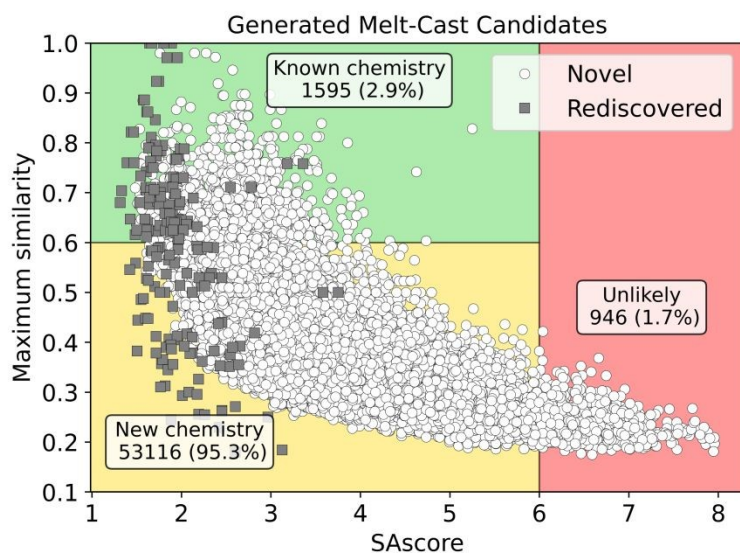


Figure 6. Distribution of maximum similarity and synthetic accessibility score (SAscore). The green region contains novel molecules with high similarity and low SAscore, indicating they are likely easy to synthesize with a potentially known synthesis route. The yellow region contains novel molecules with low similarity and low SAscore, indicating they are likely easy to synthesize but a relatively unknown synthesis route. The red region contains molecules with high SAscore that are likely hard to synthesize.

Molecules with high similarity and low SAscore are classified as high priority candidates, as they are likely synthetically accessible and may follow similar synthetic routes to known compounds. Molecules with low similarity and low SAscore are considered low priority because they are still likely synthetically accessible but may require additional effort to determine viable synthesis pathways. Molecules with SAscore values above 6 are labeled as difficult due to their synthetic complexity and are unlikely to be pursued further. We provide further comparisons of the distributions of maximum similarity and SAscore for the novel generated melt-cast candidates and the rediscovered molecules in Figure S8 of the supplemental material. Shown in Figure S8(a), the novel generated molecules display much lower maximum similarity scores with a mean less than 0.4, which has been used in prior works to indicate the novelty of generated molecules.⁹² This suggests that many of the generated melt-cast candidates are indeed novel with strong chemical distinction from known molecules. Shown in Figure S8(b), the SAScores of the



novel generated molecules are shifted higher (mean ~ 3.5) than the rediscovered (mean ~ 2) but we still find that 98.3% are below 6 indicating the vast majority are likely to be synthetically accessible.

We note that recent work using the JANUS-GA to explore molecules with high crystal heat of formation ($\Delta H_{f,s}$) and crystalline density (ρ), found that generated molecules had a distribution of SAScores shifted much higher (mean ~ 6) than what we observe in Figure 6 and Figure S8.¹⁰⁶ We speculate that because our optimization was focused on generating thermally stable molecules this may have correspondingly resulted in molecules with lower SAScore.

5. Conclusion

We developed a multi-task D-MPNN to predict fundamental properties (melting temperature, boiling temperature, decomposition temperature and vapor pressure) from the molecular graph. We deploy this model to screen known molecules and fill the gaps in the experimental data where we identify 2,532 melt-castable candidates based on thermal stability and volatility. We extend an existing genetic algorithm for dual-property optimization by implementing modifications for computing the Pareto front between two properties and use a distance metric as the fitness function. Deploying our model within this generative framework we discovered 55,745 novel melt-castable candidates, the majority of which display SAScores that suggest they can be synthetically accessible. This workflow can be readily adapted to other material properties and optimization problems. Future efforts should investigate Pareto optimization in higher-dimensional property spaces (i.e., for $n > 2$) to extend beyond dual-objective fronts.

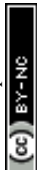
Data and Software Availability

The compiled dataset of experimental measurements, model development code and scripts for running the genetic algorithm are available at GitHub

<https://github.itap.purdue.edu/StrachanGroup/MeltCastExplore> with DOI;

<https://doi.org/10.5281/zenodo.18474595>. The source code for the modified JANUS-GA is available at GitHub <https://github.com/R-applet/JANUS> with DOI;

<https://doi.org/10.5281/zenodo.18474741>. The resulting 43 melt-cast materials from surveying experimental data, the 2,532 ML screened melt-cast materials, and the novel generated melt-cast candidates with the corresponding predicted properties are provided along the manuscript as supplemental material. A graphical user interface allowing users to make predictions and visualize the data is freely available at nanoHUB at <https://nanohub.org/tools/mcexplorer> with DOI; <https://doi.org/10.21981/TTDN-JB78>.



Author Contributions

R.J.A.: Conceptualization, Data Curation, Formal Analysis, Writing – original draft.

B.C.B.: Conceptualization, Funding Acquisition, Resources, Writing – reviewing and editing.

S.F.S.: Supervision, Funding Acquisition, Writing – reviewing and editing.

A.S.: Conceptualization, Methodology, Funding Acquisition, Resources, Writing – original draft.

Conflicts of Interest

There are no conflicts to declare.

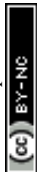
Acknowledgements

The authors thank Betsy M. Rice for useful discussion during the preparation of this manuscript.

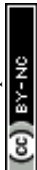
This research was sponsored in part by the Army Research Laboratory and was accomplished under Cooperative Agreement No. W911NF-20-2-0189. This research was sponsored in part by the Army Research Office and was accomplished under Cooperative Agreement No. W911NF-22-2-0170. This work was supported in part by a grant of computer time from the DoD High Performance Computing Modernization Program at the DEVCOM Army Research Laboratory.

References

1. Campbell, J. Casting. in *Complete Casting Handbook* 821–882 (Elsevier, 2015). doi:10.1016/B978-0-444-63509-9.00016-9.
2. Tadmor, Z. & Gogos, C. G. *Principles of Polymer Processing*. (John Wiley & Sons, Inc., 2006).
3. Zhou, H., Sabino, J., Yang, Y., Ward, M. D., Shtukenberg, A. G. & Kahr, B. Tailor-Made Additives for Melt-Grown Molecular Crystals: Why or Why Not? *Annu. Rev. Mater. Res.* **53**, 143–164 (2023).
4. Black, J. T. & Kohser, R. A. *DeGarmo's Materials and Processes in Manufacturing*. (Wiley, 2019).
5. Osswald, T. A. & Menges, G. Part 2: Influence of Processing on Properties: Introduction to Processing. in *Material Science of Polymers for Engineers* 161–262 (Hanser, 2012). doi:10.3139/9781569905241.
6. *ASM Handbook, Volume 15: Casting*. vol. 15 (ASM International, 2008).



7. Hu, J. & Tan, L. Polyurethane Composites and Nanocomposites for Biomedical Applications. in *Polyurethane Polymers: Composites and Nanocomposites* 477–498 (Elsevier Inc., 2017). doi:10.1016/B978-0-12-804065-2.00016-4.
8. Krasko, M. Y., Shikanov, A., Ezra, A. & Domb, A. J. Poly(ester anhydride)s prepared by the insertion of ricinoleic acid into poly(sebacic acid). *J. Polym. Sci. A Polym. Chem.* **41**, 1059–1069 (2003).
9. Basu, A. & Domb, A. J. Recent Advances in Poly(anhydride) Based Biomaterials. *Advanced Materials* **30**, 1706815 (2018).
10. Fu, X., Wang, T., Shen, W., Jiang, M., Wang, Y., Dai, Q., Wang, D., Qiu, Z., Zhang, Y., Deng, K., Zeng, Q., Zhao, N., Guo, X., Liu, Z., Liu, J. & Peng, Z. A High-Performance Carbonate-Free Lithium|Garnet Interface Enabled by a Trace Amount of Sodium. *Advanced Materials* **32**, 2000575 (2020).
11. Carlson, J. S. & Feng, P. L. Melt-cast organic glasses as high-efficiency fast neutron scintillators. *Nucl. Instrum. Methods Phys. Res. A* **832**, 152–157 (2016).
12. Schmid, S., Kast, A. K., Schröder, R. R., Bunz, U. H. F. & Melzer, C. Improved thin-film transistor performance through a melt of poly(para-phenyleneethynylene). *Macromol. Rapid Commun.* **35**, 1770–1775 (2014).
13. Rahmanudin, A., Yao, L., Jeanbourquin, X. A., Liu, Y., Sekar, A., Ripaud, E. & Sivula, K. Melt-processing of small molecule organic photovoltaics: Via bulk heterojunction compatibilization. *Green Chemistry* **20**, 2218–2224 (2018).
14. Benz, M., Delage, A., Klapötke, T. M., Kofen, M. & Stierstorfer, J. A rocky road toward a suitable TNT replacement – A closer look at three promising azoles. *Propellants, Explosives, Pyrotechnics* **48**, e202300042 (2023).
15. Ravi, P., Badgajar, D. M., Gore, G. M., Tewari, S. P. & Sikder, A. K. Review on melt cast explosives. *Propellants, Explosives, Pyrotechnics* **36**, 393–403 (2011).
16. Holbrook, E., Kroonblawd, M. P., Hamilton, B. W., Springer, H. K. & Strachan, A. Modeling Framework to Predict Melting Dynamics at Microstructural Defects in TNT-HMX High Explosive Composites. *The Journal of Physical Chemistry C* **129**, 14111–14129 (2025).
17. Forster, S. P. & Lebo, D. B. Continuous melt granulation for taste-masking of ibuprofen. *Pharmaceutics* **13**, 863 (2021).
18. Yang, Z., Hu, Y., Tang, G., Dong, M., Liu, Q. & Lin, X. Development of ibuprofen dry suspensions by hot melt extrusion: Characterization, physical stability and pharmacokinetic studies. *J. Drug Deliv. Sci. Technol.* **54**, 101313 (2019).



19. Yang, M., Wang, P., Huang, C. Y., Ku, M. S., Liu, H. & Gogos, C. Solid dispersion of acetaminophen and poly(ethylene oxide) prepared by hot-melt mixing. *Int. J. Pharm.* **395**, 53–61 (2010).
20. Paradkar, A. R., Maheshwari, M., Ketkar, A. R. & Chauhan, B. Preparation and evaluation of ibuprofen beads by melt solidification technique. *Int. J. Pharm.* **255**, 33–42 (2003).
21. Milanovic, A., Aleksic, I., Ibric, S., Parojcic, J. & Cvijic, S. Tableting of hot-melt coated paracetamol granules: Material tableting properties and quality characteristics of the obtained tablets. *European Journal of Pharmaceutical Sciences* **142**, 105121 (2020).
22. Genck, W. J., Albin, B., Baczek, F. A., Dickey, D. S., Gilbert, C. G., Herrera, T., Laros, T. J., Li, W., McCurdie, P., McGillicuddy, J. K., McNutty, T. P., Moyers, C. G., Schoenbrunn, F., Wisdom, T. W. & Chen, W. Liquid-Solid Operations and Equipment. in *Perry's Chemical Engineers' Handbook* (eds. Green, D. W. & Southard, M. Z.) 1895–2050 (New York: McGraw-Hill Education, 2019).
23. Thermodynamics Research Center (TRC). Thermodynamics Source Database. in *NIST Chemistry WebBook* (eds. Linstrom, P. J. & Mallard, W. G.) (National Institute of Standards and Technology, Gaithersburg, MD, 2025). doi:10.18434/T4D303.
24. Mansouri, K., Grulke, C. M., Richard, A. M., Judson, R. S. & Williams, A. J. An automated curation procedure for addressing chemical errors and inconsistencies in public datasets used in QSAR modelling. *SAR QSAR Environ. Res.* **27**, 939–965 (2016).
25. Bradley, J.-C., Williams, A. & Lang, A. Jean-Claude Bradley Open Melting Point Dataset. vol. 2 Preprint at <https://doi.org/doi.org/10.6084/m9.figshare.1031638.v1> (2014).
26. Wespiser, C. & Mathieu, D. Application of Machine Learning to the Design of Energetic Materials: Preliminary Experience and Comparison with Alternative Techniques. *Propellants, Explosives, Pyrotechnics* **48**, e202200264 (2023).
27. Rein, J., Meinhardt, J. M., Hofstra, J. L., Sigman, M. S. & Lin, S. A Physical Organic Approach towards Statistical Modeling of Tetrazole and Azide Decomposition. *Angewandte Chemie* **62**, e202218213 (2023).
28. Wiener, H. Structural Determination of Paraffin Boiling Points. *J. Am. Chem. Soc.* **69**, 17–20 (1947).



29. Mansouri, K., Grulke, C. M., Judson, R. S. & Williams, A. J. OPERA models for predicting physicochemical properties and environmental fate endpoints. *J. Cheminform.* **10**, 10 (2018).
30. Dixon, S. L., Duan, J., Smith, E., Von Bargen, C. D., Sherman, W. & Repasky, M. P. AutoQSAR: An automated machine learning tool for best-practice quantitative structure-activity relationship modeling. *Future Med. Chem.* **8**, 1825–1839 (2016).
31. Padiuszyński, K., Kłębowski, K. & Królikowska, M. Predicting melting point of ionic liquids using QSPR approach: Literature review and new models. *J. Mol. Liq.* **344**, 117631 (2021).
32. Zang, X., Zhou, X., Bian, H., Jin, W., Pan, X., Jiang, J., Koroleva, M. Yu. & Shen, R. Prediction and Construction of Energetic Materials Based on Machine Learning Methods. *Molecules* **28**, 322 (2022).
33. Klinger, D., Casey, A., Manship, T., Son, S. & Strachan, A. Prediction of Solid Propellant Burning Rate Characteristics Using Machine Learning Techniques. *Propellants, Explosives, Pyrotechnics* **48**, e202200267 (2023).
34. Borlido, P., Schmidt, J., Huran, A. W., Tran, F., Marques, M. A. L. & Botti, S. Exchange-correlation functionals for band gaps of solids: benchmark, reparametrization and machine learning. *NPJ Comput. Mater.* **6**, 96 (2020).
35. Gee, R. & Lindsey, R. Revolutionizing Energetic Materials Discovery and Design: The Role of Data Science and Machine Learning. *Propellants, Explosives, Pyrotechnics* **48**, e202380431 (2023).
36. Wang, S., Gong, S., Böger, T., Newnham, J. A., Vivona, D., Sokseiha, M., Gordiz, K., Aggarwal, A., Zhu, T., Zeier, W. G., Grossman, J. C. & Shao-Horn, Y. Multimodal Machine Learning for Materials Science: Discovery of Novel Li-Ion Solid Electrolytes. *Chemistry of Materials* **36**, 11541–11550 (2024).
37. Mannodi-Kanakkithodi, A. A guide to discovering next-generation semiconductor materials using atomistic simulations and machine learning. *Comput. Mater. Sci.* **243**, 113108 (2024).
38. Yang, J., Manganaris, P. & Mannodi-Kanakkithodi, A. Discovering novel halide perovskite alloys using multi-fidelity machine learning and genetic algorithm. *Journal of Chemical Physics* **160**, 064114 (2024).
39. Appleton, R. J., Salek, P., Casey, A. D., Barnes, B. C., Son, S. F. & Strachan, A. Interpretable Performance Models for Energetic Materials using Parsimonious Neural Networks. *Journal of Physical Chemistry A* **128**, 1142–1153 (2024).



40. Li, C., Verduzco, J. C., Lee, B. H., Appleton, R. J. & Strachan, A. Mapping microstructure to shock-induced temperature fields using deep learning. *NPJ Comput. Mater.* **9**, 178 (2023).
41. Chen, C. C., Appleton, R. J., Mishra, S., Nykiel, K. & Strachan, A. Discovery of new high-pressure phases – integrating high-throughput DFT simulations, graph neural networks, and active learning. *NPJ Comput. Mater.* **11**, 191 (2025).
42. Zhang, Y., Appleton, R. J., Lin, K., McCarthy, M. J., Paci, J. T., Sankaranarayanan, S. K. R. S., Strachan, A. & Espinosa, H. D. Generalizable machine learning potentials for quantum-accurate predictions of non-equilibrium behavior in 2D materials. *Comput. Methods Appl. Mech. Eng.* **448**, 118502 (2026).
43. Yap, C. W. PaDEL-descriptor: An open source software to calculate molecular descriptors and fingerprints. *J. Comput. Chem.* **32**, 1466–1474 (2011).
44. Moriwaki, H., Tian, Y. S., Kawashita, N. & Takagi, T. Mordred: A molecular descriptor calculator. *J. Cheminform.* **10**, 4 (2018).
45. Appleton, R. J., Klinger, D., Lee, B. H., Taylor, M., Kim, S., Blankenship, S., Barnes, B. C., Son, S. F. & Strachan, A. Multi-Task Multi-Fidelity Learning of Properties for Energetic Materials. *Propellants, Explosives, Pyrotechnics* **50**, e202400248 (2024).
46. Boukouvalas, Z., Puerto, M., Elton, D. C., Chung, P. W. & Fuge, M. D. Independent vector analysis for molecular data fusion: Application to property prediction and knowledge discovery of energetic materials. in *28th European Signal Processing Conference* vols 2021-January 1030–1034 (IEEE, 2021).
47. Elton, D. C., Boukouvalas, Z., Butrico, M. S., Fuge, M. D. & Chung, P. W. Applying machine learning techniques to predict the properties of energetic materials. *Sci. Rep.* **8**, 9059 (2018).
48. Barnes, B. C., Elton, D. C., Boukouvalas, Z., Taylor, D. E., Mattson, W. D., Fuge, M. D. & Chung, P. W. Machine Learning of Energetic Material Properties. in *Proceedings of the 16th International Detonation Symposium* (2018). doi:10.48550/arXiv.1807.06156.
49. Sun, M., Zhao, S., Gilvary, C., Elemento, O., Zhou, J. & Wang, F. Graph convolutional networks for computational drug development and discovery. *Brief. Bioinform.* **21**, 919–935 (2020).



50. Liu, K., Sun, X., Jia, L., Ma, J., Xing, H., Wu, J., Gao, H., Sun, Y., Boulnois, F. & Fan, J. Chemi-net: A molecular graph convolutional network for accurate drug property prediction. *Int. J. Mol. Sci.* **20**, 3389 (2019).
51. Rahman, M. H., Gollapalli, P., Manganaris, P., Yadav, S. K., Pilia, G., DeCost, B., Choudhary, K. & Mannodi-Kanakkithodi, A. Accelerating defect predictions in semiconductors using graph neural networks. *APL Machine Learning* **2**, 016122 (2024).
52. Yang, K., Swanson, K., Jin, W., Coley, C., Eiden, P., Gao, H., Guzman-Perez, A., Hopper, T., Kelley, B., Mathea, M., Palmer, A., Settels, V., Jaakkola, T., Jensen, K. & Barzilay, R. Analyzing Learned Molecular Representations for Property Prediction. *J. Chem. Inf. Model.* **59**, 3370–3388 (2019).
53. Heid, E., Greenman, K. P., Chung, Y., Li, S. C., Graff, D. E., Vermeire, F. H., Wu, H., Green, W. H. & McGill, C. J. Chemprop: A Machine Learning Package for Chemical Property Prediction. *J. Chem. Inf. Model.* **64**, 9–17 (2024).
54. Gasteiger, J., Groß, J. & Günnemann, S. Directional Message Passing for Molecular Graphs. in *International Conference on Learning Representations* (2020). doi:10.48550/arXiv.2003.03123.
55. Zhang, S., Liu, Y. & Xie, L. Molecular Mechanics-Driven Graph Neural Network with Multiplex Graph for Molecular Structures. <http://arxiv.org/abs/2011.07457> (2020).
56. Chen, C., Ye, W., Zuo, Y., Zheng, C. & Ong, S. P. Graph Networks as a Universal Machine Learning Framework for Molecules and Crystals. *Chemistry of Materials* **31**, 3564–3572 (2019).
57. Appleton, R. J., Barnes, B. C. & Strachan, A. Data Fusion of Deep Learned Molecular Embeddings for Property Prediction. *J. Chem. Inf. Model.* **65**, 11620–11630 (2025).
58. Gómez-Bombarelli, R., Wei, J. N., Duvenaud, D., Hernández-Lobato, J. M., Sánchez-Lengeling, B., Sheberla, D., Aguilera-Iparraguirre, J., Hirzel, T. D., Adams, R. P. & Aspuru-Guzik, A. Automatic Chemical Design Using a Data-Driven Continuous Representation of Molecules. *ACS Cent. Sci.* **4**, 268–276 (2018).
59. Jin, W., Yang, K., Barzilay, R. & Jaakkola, T. Learning Multimodal Graph-to-Graph Translation for Molecular Optimization. <http://arxiv.org/abs/1812.01070> (2018).



60. Assouel, R., Ahmed, M., Segler, M. H., Saffari, A. & Bengio, Y. DEFactor: Differentiable Edge Factorization-based Probabilistic Graph Generation. <http://arxiv.org/abs/1811.09766> (2018).
61. Liu, Q., Allamanis, M., Brockschmidt, M. & Gaunt, A. L. Constrained Graph Variational Autoencoders for Molecule Design. in *Advances in neural information processing systems 31* (2018).
62. Jin, W., Barzilay, R. & Jaakkola, T. Junction Tree Variational Autoencoder for Molecular Graph Generation. in *Proceedings of the 35th International Conference on Machine Learning* 2323–2332 (2018).
63. Ochiai, T., Inukai, T., Akiyama, M., Furui, K., Ohue, M., Matsumori, N., Inuki, S., Uesugi, M., Sunazuka, T., Kikuchi, K., Takeya, H. & Sakakibara, Y. Variational autoencoder-based chemical latent space for large molecular structures with 3D complexity. *Commun. Chem.* **6**, 249 (2023).
64. Kusner, M. J., Paige, B. & Miguel Hernández-Lobato, J. Grammar Variational Autoencoder. in *Proceedings of the 34th International Conference on Machine Learning* 1945–1954 (2017).
65. Lim, J., Hwang, S. Y., Moon, S., Kim, S. & Kim, W. Y. Scaffold-based molecular design with a graph generative model. *Chem. Sci.* **11**, 1153–1164 (2020).
66. Pathak, Y., Juneja, K. S., Varma, G., Ehara, M. & Priyakumar, U. D. Deep learning enabled inorganic material generator. *Physical Chemistry Chemical Physics* **22**, 26935–26943 (2020).
67. Boitreaud, J., Mallet, V., Oliver, C. & Waldispühl, J. OptiMol: Optimization of Binding Affinities in Chemical Space for Drug Discovery. *J. Chem. Inf. Model.* **60**, 5658–5666 (2020).
68. Yao, Z., Sánchez-Lengeling, B., Bobbitt, N. S., Bucior, B. J., Kumar, S. G. H., Collins, S. P., Burns, T., Woo, T. K., Farha, O. K., Snurr, R. Q. & Aspuru-Guzik, A. Inverse design of nanoporous crystalline reticular materials with deep generative models. *Nat. Mach. Intell.* **3**, 76–86 (2021).
69. Maziarka, Ł., Pocha, A., Kaczmarczyk, J., Rataj, K., Danel, T. & Warchoł, M. Mol-CycleGAN: A generative model for molecular optimization. *J. Cheminform.* **12**, 2 (2020).
70. De Cao, N. & Kipf, T. MolGAN: An implicit generative model for small molecular graphs. <http://arxiv.org/abs/1805.11973> (2018).



71. Guimaraes, G. L., Sanchez-Lengeling, B., Outeiral, C., Farias, P. L. C. & Aspuru-Guzik, A. Objective-Reinforced Generative Adversarial Networks (ORGAN) for Sequence Generation Models. <http://arxiv.org/abs/1705.10843> (2017).
72. Park, J., Lee, Y. & Kim, J. Multi-modal conditional diffusion model using signed distance functions for metal-organic frameworks generation. *Nature Communications* **16**, 34 (2025).
73. Runcie, N. T. & Mey, A. S. J. S. SILVR: Guided Diffusion for Molecule Generation. *J. Chem. Inf. Model.* **63**, 5996–6005 (2023).
74. Huang, L., Xu, T., Yu, Y., Zhao, P., Chen, X., Han, J., Xie, Z., Li, H., Zhong, W., Wong, K. C. & Zhang, H. A dual diffusion model enables 3D molecule generation and lead optimization based on target pockets. *Nat. Commun.* **15**, 2657 (2024).
75. Alakhdar, A., Poczos, B. & Washburn, N. Diffusion Models in De Novo Drug Design. *J. Chem. Inf. Model.* **64**, 7238–7256 (2024).
76. Chen, C. C., Appleton, R. J., Nykiel, K., Mishra, S., Yao, S. & Strachan, A. How accurate is density functional theory at high pressures? *Comput. Mater. Sci.* **247**, 113458 (2025).
77. Biermair, F., Razumovskiy, V. I. & Ressel, G. Influence of alloying on thermodynamic properties of AlCoCrFeNiTi high entropy alloys from DFT calculations. *Comput. Mater. Sci.* **202**, 110952 (2022).
78. Kumar, A., Ali, Z. A. & Wong, B. M. Efficient predictions of formation energies and convex hulls from density functional tight binding calculations. *J. Mater. Sci. Technol.* **141**, 236–244 (2023).
79. Nykiel, K. & Strachan, A. High-throughput density functional theory screening of double transition metal MXene precursors. *Sci. Data* **10**, 827 (2023).
80. Karumuri, S., Hernandez, A., Mishra, S., McClure, Z., Tucker, V., Flanagan, J. C., Hwang, S., Sandhage, K. H., Billionis, I., Titus, M. S. & Strachan, A. Design of high-hardness complex concentrated alloys from physics, machine learning, and experiments. *J. Appl. Phys.* **138**, 085106 (2025).
81. Slater, T. & Timms, D. Meeting on binding sites: Characterizing and satisfying steric and chemical restraints. *J. Mol. Graph.* **11**, 248–251 (1993).
82. Westhead, D. R., Clark, D. E., Frenkel, D., Li, J., Murray, C. W., Robson, B. & Waszkowycz, B. PRO_LIGAND: An approach to de novo molecular design. 3. A genetic algorithm for structure refinement. *J. Comput. Aided. Mol. Des.* **9**, 139–148 (1995).



83. Glen, R. C. & Payne, W. R. A genetic algorithm for the automated generation of molecules within constraints. *J. Comput. Aided. Mol. Des.* **9**, 181–202 (1995).
84. Weininger, D. Smiles, a chemical language and information system. 1. introduction to methodology and encoding rules. *J. Chem. Inf. Comput. Sci.* **28**, 31–36 (1988).
85. Weininger, D., Weininger, A. & Weininger, J. L. Smiles. 2. algorithm for generation of unique smiles notation. *J. Chem. Inf. Comput. Sci.* **29**, 97–101 (1989).
86. Polishchuk, P. CReM: Chemically reasonable mutations framework for structure generation. *J. Cheminform.* **12**, 28 (2020).
87. Leguy, J., Cauchy, T., Glavatskikh, M., Duval, B. & Da Mota, B. EvoMol: a flexible and interpretable evolutionary algorithm for unbiased de novo molecular generation. *J. Cheminform.* **12**, 55 (2020).
88. Kwon, Y. & Lee, J. MolFinder: an evolutionary algorithm for the global optimization of molecular properties and the extensive exploration of chemical space using SMILES. *J. Cheminform.* **13**, 24 (2021).
89. Jensen, J. H. A graph-based genetic algorithm and generative model/Monte Carlo tree search for the exploration of chemical space. *Chem. Sci.* **10**, 3567–3572 (2019).
90. Krenn, M., Häse, F., Nigam, A. K., Friederich, P. & Aspuru-Guzik, A. Self-referencing embedded strings (SELFIES): A 100% robust molecular string representation. *Mach. Learn. Sci. Technol.* **1**, 045024 (2020).
91. Nigam, A., Pollice, R., Krenn, M., Gomes, G. D. P. & Aspuru-Guzik, A. Beyond generative models: Superfast traversal, optimization, novelty, exploration and discovery (STONED) algorithm for molecules using SELFIES. *Chem. Sci.* **12**, 7079–7090 (2021).
92. Nigam, A. K., Pollice, R. & Aspuru-Guzik, A. Parallel tempered genetic algorithm guided by deep neural networks for inverse molecular design. *Digital Discovery* **1**, 390–404 (2022).
93. Kim, S., Chen, J., Cheng, T., Gindulyte, A., He, J., He, S., Li, Q., Shoemaker, B. A., Thiessen, P. A., Yu, B., Zaslavsky, L., Zhang, J. & Bolton, E. E. PubChem 2023 update. *Nucleic Acids Res.* **51**, D1373–D1380 (2023).
94. SciFinder. <https://scifinder-n.cas.org/>.
95. Landrum, G. RDKit: Open-source cheminformatics. Preprint at <https://doi.org/10.5281/zenodo.591637> (2023).



96. Lansford, J. L., Jensen, K. F. & Barnes, B. C. Physics-informed Transfer Learning for Out-of-sample Vapor Pressure Predictions. *Propellants, Explosives, Pyrotechnics* **48**, e202200265 (2023).
97. Hansmann, U. H. E. Parallel tempering algorithm for conformational studies of biological molecules. *Chem. Phys. Lett.* **281**, 140–150 (1997).
98. Earl, D. J. & Deem, M. W. Parallel tempering: Theory, applications, and new perspectives. *Physical Chemistry Chemical Physics* **7**, 3910–3916 (2005).
99. Galeazzo, T. & Shiraiwa, M. Predicting glass transition temperature and melting point of organic compounds via machine learning and molecular embeddings. *Environmental Science: Atmospheres* **2**, 362–374 (2022).
100. Schroeder, D. V. *An Introduction to Thermal Physics*. (Oxford University Press, 2000).
101. Swain, M. PubChemPy: A Python Wrapper for the PubChem API. <https://pubchempy.readthedocs.io/en/latest/index.html>.
102. Swain, M. CIRpy: A Python Library for Chemical Information Retrieval. <https://cirpy.readthedocs.io/en/latest/index.html>.
103. Rogers, D. J. & Tanimoto, T. T. A Computer Program for Classifying Plants: The computer is programmed to simulate the taxonomic process of comparing each case with every other case. *Science (1979)*. **132**, 1115–1118 (1960).
104. Chithrananda, S., Grand, G. & Ramsundar, B. ChemBERTa: Large-Scale Self-Supervised Pretraining for Molecular Property Prediction. <http://arxiv.org/abs/2010.09885> (2020).
105. Ertl, P. & Schuffenhauer, A. Estimation of synthetic accessibility score of drug-like molecules based on molecular complexity and fragment contributions. *J. Cheminform.* **1**, 8 (2009).
106. Antoniuk, E., Li, P., Keilbart, N., Weitzner, S., Kailkhura, B. & Hiszpanski, A. M. Active Learning Enables Extrapolation in Molecular Generative Models. <https://doi.org/10.48550/arXiv.2501.02059> (2025).



Data and Software Availability

The compiled dataset of experimental measurements, model development code and scripts for running the genetic algorithm are available at GitHub

<https://github.itap.purdue.edu/StrachanGroup/MeltCastExplore> with DOI;

<https://doi.org/10.5281/zenodo.18474595>. The source code for the modified JANUS-GA is

available at GitHub <https://github.com/R-applet/JANUS> with DOI;

<https://doi.org/10.5281/zenodo.18474741>. The resulting 43 melt-cast materials from surveying experimental data, the 2,532 ML screened melt-cast materials, and the novel generated melt-cast candidates with the corresponding predicted properties are provided along the manuscript as supplemental material. A graphical user interface allowing users to make predictions and visualize the data is freely available at nanoHUB at <https://nanohub.org/tools/mcexplorer> with DOI; <https://doi.org/10.21981/TTDN-JB78>.

